Available online at www.sciencedirect.com
SCIENCE DIRECT®
ELSEVIER
International Journal of Solids and Structures 43 (2006) 307–324
INTERNATIONAL JOURNAL OF SOLIDS and STRUCTURES
www.elsevier.com/locate/ijsolstr

Thermo-mechanical post-buckling of FGM cylindrical panels with temperature-dependent properties

J. Yang [a], K.M. Liew [b], Y.F. Wu [a], S. Kitipornchai [a,*]

[a] *Department of Building and Construction, City University of Hong Kong, Tat Chee Avenue, Kowloon, Hong Kong*
[b] *Nanyang Centre for Supercomputing and Visualization, School of Mechanical and Production Engineering, Nanyang Technological University, Nanyang Avenue, Singapore 639798, Singapore*

Received 27 August 2004; received in revised form 1 April 2005
Available online 23 May 2005

Abstract

This paper presents thermo-mechanical post-buckling analysis of cylindrical panels that are made of functionally graded materials (FGMs) with temperature-dependent thermo-elastic properties that are graded in the direction of thickness according to a simple power law distribution in terms of the volume fractions of the constituents. The panel is initially stressed by an axial load, and is then subjected to a uniform temperature change. The theoretical formulations are based on the classical shell theory with von-Karman–Donnell-type nonlinearity. The effect of initial geometric imperfection is also included. A differential quadrature (DQ) based semi-analytical method combined with an iteration process is employed to predict the critical buckling load (where it is applicable) and to trace the post-buckling equilibrium path of FGM cylindrical panels under thermo-mechanical loading. Numerical results are presented for panels with silicon nitride and nickel as the ceramic and metal constituents. The effects of temperature-dependent properties, volume fraction index, axial load, initial imperfection, panel geometry and boundary conditions on the thermo-mechanical post-buckling behavior are evaluated in detail through parametric studies.

Keywords: Thermo-mechanical post-buckling; Functionally graded materials; Temperature-dependent properties; Cylindrical panel

1. Introduction

Due to their unique advantages of being able to withstand severe high-temperature environment while maintaining structural integrity, microscopically inhomogeneous functionally graded materials (FGM),

* Corresponding author. Tel.: +852 2788 8028; fax: +852 2788 7612.
E-mail address: bcskit@cityu.edu.hk (S. Kitipornchai).

0020-7683/$ - see front matter © 2005 Elsevier Ltd. All rights reserved.
doi:10.1016/j.ijsolstr.2005.04.001

whose material properties vary smoothly and continuously from one surface to the other by gradually changing the volume fraction of their constituent materials, have received considerable attention in many industries, especially in high-temperature applications such as space shuttle, aircraft, nuclear reactors and etc., as is reflected in a great number of research papers published on this subject (e.g., Koizumi, 1993; Tanigawa, 1995; Aboudi et al., 1997; Reddy and Chin, 1998; Noda, 1999; Reddy, 2000; Reddy and Cheng, 2001; Liew et al., 2001b, 2002, 2003a,b, 2004; Ng et al., 2002; Vel and Batra, 2002; Kitipornchai et al., 2004; Yang and Shen, 2003a,b; Yang et al., 2003, 2004a,b). When FGMs are used as heat-shielding components with restrains against in-plane thermal expansions or contractions, significant thermally induced strains and stresses develop at elevated temperatures, which introduce a certain membrane pre-stress state that may initiate buckling and post-buckling (Javaheri and Eslami, 2002; Morimoto et al., 2003; Ma and Wang, 2003; Na and Kim, 2004). It is further envisaged that considerable variation in the material properties with temperature fluctuations makes the mechanical response even more complicated, which calls for a thorough understanding of the buckling and post-buckling behavior of FGMs with temperature-dependent material properties being taken into account.

Numerous investigations of the buckling and post-buckling responses of composite structures in thermal environments can be found in the literature, among which those incorporating temperature-dependent material properties are due to Chen and Chen (1989), Noor and Burton (1992a,b), Argyris and Tenek (1995), Feldman (1996), Deng et al. (2000), Lee (2001), Shen (2001) and Singha et al. (2003). Significant influence of temperature-dependent properties on the critical buckling temperature and post-buckling temperature–deflection curves has been reported. For FGM shell structures, studies on the buckling and post-buckling behavior under different thermal and compressive loading are limited in number. Shahsiah and Eslami (2003) discussed the instability of FGM cylindrical shells under two types of thermal loads based on the first order shell theory and the complete Sanders kinematic equations. Sofiyev (2004) dealt with the stability analysis of FGM truncated conical shells that are subjected to a uniform external pressure which is a power function of time. A Lagrange–Hamilton type variational principle was employed to solve the governing differential equations. In his work on the stability of functionally graded shape memory alloy sandwich panels that are subjected to the simultaneous action of a uniform temperature and a uniaxial compression, Birman (1997) found that, at elevated temperatures, the buckling load can be increased by using shape memory alloy (SMA) fibers in resin sleeves embedded within the core, at the midplane of the sandwich panel. When dealing with the post-buckling behavior of FGM shells, geometrically nonlinear kinematics will be involved and the analysis becomes much more complex. Shen (2002a,b, 2003) and Shen and Leung (2003) conducted a series of studies on the post-buckling of FGM cylindrical shells and cylindrical panels under pressure or axial compression. The effect of initial geometric imperfection was included in the analyses. Woo et al. (2003) presented an analytical solution for the post-buckling of FGM thin plates and shallow cylindrical shells under edge compression combined with a uniform temperature field by using mixed Fourier series. The above-mentioned work can be divided into two types: The first type (those by Shahsiah and Eslami, 2003 and Woo et al., 2003) gave the thermal buckling or post-buckling analysis but the temperature-dependence of the material properties was not considered whereas the second type (those by Shen, 2002a,b, 2003; Shen and Leung, 2003; Sofiyev, 2004) used temperature-dependent material properties in compressive buckling or post-buckling analyses only. Within the framework of classical shell theory with von Karman–Donnell-type of kinematic nonlinearity, Shen (2004) recently investigated the thermal post-buckling behavior of imperfect FGM cylindrical thin shells of finite length. The material properties were assumed to be nonlinearly dependent on the temperature, and a singular perturbation technique, together with an iteration process, was used to determine the buckling temperature and post-buckling temperature–deflection curves. Numerical results were presented for cylindrical shells that are made from two sets of material mixtures under a uniform temperature change. In the aforementioned studies, the loading condition is either thermal or mechanical. The effect of a combined thermo-mechanical loading was not considered. To the best of our knowledge, no studies have been reported in the literature

that concern the post-buckling behavior of functionally graded cylindrical panels with temperature-dependent material properties and subjected to a combined action of thermal and mechanical loadings.

In this paper, the thermo-mechanical buckling and post-buckling of functionally graded cylindrical thin panels are investigated by using the classical shell theory. The material properties, which are modeled as nonlinear functions of the temperature, are assumed to vary smoothly along the thickness direction according to a power law distribution of the constituent materials. The theoretical formulations include the effects of thermal loads, initial geometric imperfection, and von-Karman–Donnell-type nonlinearity which considers moderate deflections and small strains. The panel is subjected to a combined initial axial force and a uniform temperature change. Nonlinear governing differential equations are derived in terms of transverse deflection and stress function and are then transformed into a nonlinear algebraic system through a semi-analytical differential quadrature-Galerkin method followed by an iteration process that determines the buckling temperature and the post-buckling equilibrium path of FGM cylindrical panels under simply supported, clamped, or mixed boundary conditions. Numerical results are provided for cylindrical panels made from silicon nitride and nickel to show the influence of temperature-dependent material properties, initial axial load, material composition, geometric imperfection, panel geometry, and boundary conditions on the thermo-mechanical buckling and post-buckling response of FGM cylindrical panels.

2. Theoretical formulations

Consider an FGM cylindrical thin panel with radius of curvature R, thickness h, axial length L and arc length S that is subjected to an axial load p_x combined with a uniform temperature change ΔT. The panel is made from a mixture of ceramics and metals, and is defined in a coordinate system (X, θ, Z), as is shown in Fig. 1, where X and θ are in the axial and circumferential directions of the panel and Z is perpendicular to the middle surface and points inwards. Suppose that the material composition of the panel varies smoothly along the thickness in such a way that the inner surface is metal-rich and the outer surface is ceramic-rich by following a simple power law in terms of the volume fractions of the constituents as

$$V_c = \left(\frac{2Z+h}{2h}\right)^n, \quad V_m = 1 - \left(\frac{2Z+h}{2h}\right)^n \tag{1}$$

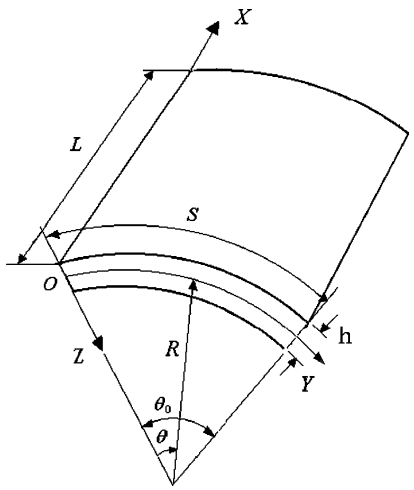

Fig. 1. Configuration and the coordinate system of the FGM cylindrical panel.

where V_c and V_m are the ceramic and metal volume fractions and volume fraction index n is a nonnegative integer that defines the material distribution and can be chosen to optimize the structural response. The effective properties P_{eff}, such as Young's modulus E, Poisson's ratio v, and the coefficient of thermal expansion α, can be determined by

$$P_{eff} = P_m + (P_c - P_m)V_c \tag{2}$$

in which the subscripts "c" and "m" stand for ceramic and metal, respectively.

As FGMs are most commonly used in high temperature environments in which significant changes in material properties are to be expected, the material properties of an FGM cylindrical panel are both position and temperature dependent. For example, Young's modulus usually decreases, and the thermal expansion coefficient usually increases at elevated temperatures (Noor and Burton, 1992b). It is essential to account for this temperature-dependence for reliable and accurate prediction of the structural response. Without loss of generality, the material properties are expressed as the nonlinear functions of environment temperature T (K) (Touloukian, 1967)

$$P = P_0(P_{-1}T^{-1} + 1 + P_1T + P_2T^2 + P_3T^3) \tag{3}$$

in which $T = T_0 + \Delta T$ and $T_0 = 300$ K (room temperature), and P_0, P_{-1}, P_1, P_2, and P_3 are temperature-dependent coefficients that are unique to the constituent materials. Thus, Young's modulus E, Poisson's ratio v, and the coefficient of thermal expansion α can be written from Eqs. (1)–(3) as

$$\begin{aligned} E &= (E_c - E_m)\left(\frac{2Z+h}{2h}\right)^n + E_m \\ v &= (v_c - v_m)\left(\frac{2Z+h}{2h}\right)^n + v_m \\ \alpha &= (\alpha_c - \alpha_m)\left(\frac{2Z+h}{2h}\right)^n + \alpha_m \end{aligned} \tag{4}$$

It is evident that $E = E_c$, $v = v_c$, $\alpha = \alpha_c$ at $Z = h/2$ and $E = E_m$, $v = v_m$, $\alpha = \alpha_m$ at $Z = -h/2$.

Let $(\overline{U}, \overline{V}, \overline{W})$ be the displacement components in the (X, θ, Z) coordinates. The panel is assumed to be initially imperfect with geometric imperfection $\overline{W}^*$, and $\overline{W}$ is the additional deflection that is caused by thermo-mechanical loading. Denote the stress function by $\overline{F}(X, \theta)$ which is related to the stress resultants by $\overline{N}_x = \dfrac{\partial^2 \overline{F}}{R^2 \partial \theta^2}$, $\overline{N}_\theta = \dfrac{\partial^2 \overline{F}}{\partial X^2}$, $\overline{N}_{x\theta} = -\dfrac{\partial^2 \overline{F}}{R\,\partial X\,\partial \theta}$, and introduce the following dimensionless quantities:

$$\begin{aligned} &x = \frac{X}{L}, \quad \beta = \frac{L}{R}, \quad (W, W^*) = \frac{(\overline{W}, \overline{W}^*)}{(D_{11}^* D_{22}^* A_{11}^* A_{22}^*)^{1/4}}, \quad F = \frac{\overline{F}}{\sqrt{(D_{11}^* D_{22}^*)}}, \quad \lambda_1 = \frac{p_x R^2}{\sqrt{(D_{11}^* D_{22}^*)}} \\ &\gamma_{12} = \frac{D_{12}^* + 2D_{66}^*}{D_{11}^*}, \quad \gamma_{14} = \left(\frac{D_{22}^*}{D_{11}^*}\right)^{1/2}, \quad \gamma_{22} = \frac{A_{12}^* + 0.5A_{66}^*}{A_{22}^*}, \quad \gamma_{24} = \left(\frac{A_{11}^*}{A_{22}^*}\right)^{1/2}, \quad \gamma_5 = \frac{A_{12}^*}{A_{22}^*} \\ &(\gamma_{30}, \gamma_{32}, \gamma_{34}) = \frac{1}{(D_{11}^* D_{22}^* A_{11}^* A_{22}^*)^{1/4}}\left(B_{21}^*, B_{11}^* + B_{22}^* - 2B_{66}^*, B_{12}^*\right), \quad \xi = \frac{L}{(D_{11}^* D_{22}^* A_{11}^* A_{22}^*)^{1/4}} \\ &(\gamma_{M11}, \gamma_{M12}, \gamma_{M21}) = \frac{1}{(A_{11}^* A_{22}^* D_{11}^* D_{22}^*)^{1/4}}(B_{21}^*, B_{11}^*, B_{22}^*), \quad (\gamma_{M13}, \gamma_{M22}) = \frac{1}{D_{11}^*}(D_{21}^*, D_{12}^*) \end{aligned} \tag{5}$$

Based on the classical shell theory and von-Karman–Donnell-type kinematic relations, the dimensionless governing equations for an FGM cylindrical panel under mid-plane loading and a uniform temperature change can be derived as follows:

$$L_{11}(W)+L_{12}(F)-\gamma_{14}\beta\xi\frac{\partial^2 F}{\partial x^2}=\gamma_{14}\beta^2 L(W+W^*,F) \tag{6}$$

$$L_{21}(W)+L_{22}(F)-\gamma_{24}\beta\xi\frac{\partial^2 W}{\partial x^2}=-\frac{1}{2}L(W+2W^*,W) \tag{7}$$

where the partial differential operators are

$$\begin{aligned}
L_{11}(\ ) &= \frac{\partial^4}{\partial x^4}+2\gamma_{12}\beta^2\frac{\partial^4}{\partial x^2\,\partial\theta^2}+\gamma_{14}^2\beta^4\frac{\partial^4}{\partial\theta^4}\\
L_{12}(\ ) &= \gamma_{14}\left(\gamma_{30}\frac{\partial^4}{\partial x^4}+\gamma_{32}\beta^2\frac{\partial^4}{\partial x^2\,\partial\theta^2}+\gamma_{34}\beta^4\frac{\partial^4}{\partial\theta^4}\right)\\
L_{21}(\ ) &= -\gamma_{24}\left(\gamma_{30}\frac{\partial^4}{\partial x^4}+\gamma_{32}\beta^2\frac{\partial^4}{\partial x^2\,\partial\theta^2}+\gamma_{34}\beta^4\frac{\partial^4}{\partial\theta^4}\right)\\
L_{22}(\ ) &= \frac{\partial^4}{\partial x^4}+2\gamma_{22}\beta^2\frac{\partial^4}{\partial x^2\,\partial\theta^2}+\gamma_{24}^2\beta^4\frac{\partial^4}{\partial\theta^4}-\beta\xi\frac{\partial^2}{\partial x^2}\\
L(\ ) &= \frac{\partial^2}{\partial x^2}\frac{\partial^2}{\partial\theta^2}-2\frac{\partial^2}{\partial x\,\partial\theta}\frac{\partial^2}{\partial x\,\partial\theta}+\frac{\partial^2}{\partial\theta^2}\frac{\partial^2}{\partial x^2}
\end{aligned} \tag{8}$$

The reduced stiffness elements A^*_{ij}, B^*_{ij}, and D^*_{ij} are calculated from

$$A^*=A^{-1},\quad B^*=-A^{-1}B,\quad D^*=D-BA^{-1}B \tag{9}$$

and

$$(A_{ij},B_{ij},D_{ij})=\int_{-h/2}^{h/2}(Q_{ij})(1,Z,Z^2)\,\mathrm{d}Z\quad(i,j=1,2,6) \tag{10}$$

For FGMs with temperature-dependent material properties, the elastic stiffness Q_{ij} are dependent on both temperature and position.

The dimensionless moment resultants $(M_x, M_\theta, M_{x\theta})$ are

$$M_x=-\gamma_{14}\left(\gamma_{M11}\frac{\partial^2 F}{\partial x^2}+\gamma_{M12}\beta^2\frac{\partial^2 F}{\partial\theta^2}\right)-\left(\frac{\partial^2 W}{\partial x^2}+\gamma_{M13}\beta^2\frac{\partial^2 W}{\partial\theta^2}\right)+M_x^{\mathrm{T}} \tag{11a}$$

$$M_\theta=-\gamma_{14}\left(\gamma_{M21}\frac{\partial^2 F}{\partial x^2}+\gamma_{34}\beta^2\frac{\partial^2 F}{\partial\theta^2}\right)-\left(\gamma_{M22}\frac{\partial^2 W}{\partial x^2}+\gamma_{14}^2\beta^2\frac{\partial^2 W}{\partial\theta^2}\right)+M_\theta^{\mathrm{T}} \tag{11b}$$

$$M_{x\theta}=-\gamma_{14}\left(\gamma_{M31}\frac{\partial^2 F}{\partial x^2}+\gamma_{M32}\beta^2\frac{\partial^2 F}{\partial\theta^2}\right)-\left(\gamma_{M33}\frac{\partial^2 W}{\partial x^2}+\gamma_{M34}\beta^2\frac{\partial^2 W}{\partial\theta^2}\right)+M_{x\theta}^{\mathrm{T}} \tag{11c}$$

where

$$(M_x^{\mathrm{T}},M_\theta^{\mathrm{T}},M_{x\theta}^{\mathrm{T}})=(\overline{M}_x^{\mathrm{T}},\overline{M}_\theta^{\mathrm{T}},\overline{M}_{x\theta}^{\mathrm{T}})L^2/D_{11}^*(A_{11}^*A_{22}^*D_{11}^*D_{22}^*)^{1/4} \tag{12}$$

The thermal force resultants $(\overline{N}_x^{\mathrm{T}},\overline{N}_\theta^{\mathrm{T}},\overline{N}_{x\theta}^{\mathrm{T}})$ and moment resultants $(\overline{M}_x^{\mathrm{T}},\overline{M}_\theta^{\mathrm{T}},\overline{M}_{x\theta}^{\mathrm{T}})$ are given by

$$\begin{bmatrix}\overline{N}_x^{\mathrm{T}} & \overline{M}_x^{\mathrm{T}}\\ \overline{N}_\theta^{\mathrm{T}} & \overline{M}_\theta^{\mathrm{T}}\\ \overline{N}_{x\theta}^{\mathrm{T}} & \overline{M}_{x\theta}^{\mathrm{T}}\end{bmatrix}=-\int_{-h/2}^{h/2}\begin{bmatrix}Q_{11} & Q_{12} & Q_{16}\\ Q_{12} & Q_{22} & Q_{26}\\ Q_{16} & Q_{26} & Q_{66}\end{bmatrix}\begin{bmatrix}1 & 0\\ 0 & 1\\ 0 & 0\end{bmatrix}\begin{Bmatrix}\alpha\\ \alpha\end{Bmatrix}(1,Z)\Delta T\,\mathrm{d}Z \tag{13}$$

The panel may be either simply supported or clamped on each of its edges. The associated out-of-plane boundary conditions read

$$\text{Simply supported (S)}: W = 0;\ \ M_x = 0 \ \text{ or } \ M_\theta = 0 \tag{14a}$$

$$\text{Clamped (C)}: W = 0;\ \ \frac{\partial W}{\partial x} = 0 \ \text{ or } \ \frac{\partial W}{\partial \theta} = 0 \tag{14b}$$

Depending on the nature of constraints against mid-plane displacements, the following cases of in-plane boundary conditions, referred to as Case 1 and Case 2 respectively, are considered in the analysis:

Case 1: The uniform axial load is applied on the curved edges $x = 0, 1$. The panel is freely movable in the x-direction but is immovable at the unloaded straight edges $\theta = 0, \theta_0$.
Case 2: The panel is fully immovable at all edges.

The in-plane boundary conditions require that

$$\frac{\partial^2 F}{\partial x\,\partial \theta} = 0; \quad \int_0^{\theta_0} \frac{\partial^2 F}{\partial \theta^2}\,\mathrm{d}\theta + \lambda_1 = 0 \ \text{ or } \ V = 0 \ \text{(Case 1)} \tag{15a}$$

or

$$\frac{\partial^2 F}{\partial x\,\partial \theta} = 0; \quad U = 0 \ \text{ or } \ V = 0 \ \text{(Case 2)} \tag{15b}$$

in which

$$U = \frac{1}{\beta}\int_0^{\theta_0}\int_0^1 \left[\beta^2\gamma_{24}^2\frac{\partial^2 F}{\partial \theta^2} + \gamma_5\frac{\partial^2 F}{\partial x^2} - \gamma_{24}\left(\gamma_{M12}\frac{\partial^2 W}{\partial x^2} + \gamma_{34}\beta^2\frac{\partial^2 W}{\partial \theta^2}\right)\right.$$
$$\left. -\gamma_{24}\left(0.5\frac{\partial^2 W}{\partial x^2} + \frac{\partial W}{\partial x}\frac{\partial W^*}{\partial x}\right) - (\gamma_{24}^2 N_x^{\mathrm{T}} + \gamma_5 N_\theta^{\mathrm{T}})\right] \tag{16a}$$

$$V = \frac{1}{\beta}\int_0^{\theta_0}\int_0^1 \left[\frac{\partial^2 F}{\partial x^2} + \gamma_5\beta^2\frac{\partial^2 F}{\partial \theta^2} - \gamma_{24}\left(\gamma_{30}\frac{\partial^2 W}{\partial x^2} + \gamma_{M21}\beta^2\frac{\partial^2 W}{\partial \theta^2}\right) - \gamma_{24}\beta^2\left(0.5\frac{\partial^2 W}{\partial \theta^2} + \frac{\partial W}{\partial \theta}\frac{\partial W^*}{\partial \theta}\right)\right.$$
$$\left. +\gamma_{24}\xi\beta W - (\gamma_5 N_x^{\mathrm{T}} + N_\theta^{\mathrm{T}})\right] \tag{16b}$$

where $(N_x^{\mathrm{T}}, N_\theta^{\mathrm{T}}, N_{x\theta}^{\mathrm{T}}) = (\overline{N}_x^{\mathrm{T}}, \overline{N}_\theta^{\mathrm{T}}, \overline{N}_{x\theta}^{\mathrm{T}})L^2/\sqrt{(D_{11}^* D_{22}^*)}$.

It is worth noting that the thermal effect terms, which vanish in the governing equations (6) and (7) due to the uniform distribution of ΔT, are present in the boundary conditions (14) and (15).

3. Solution procedures

The governing equations (6) and (7) together with the boundary conditions (14) and (15) form a nonlinear partial differential system that is also dependent on temperature. A differential quadrature (DQ)-based semi-analytical iteration approach is used to solve this nonlinear system. The essence of this method is first to convert the partial differential equations into a set of ordinary differential equations by making use of DQ approximation, and then to apply the Galerkin technique to obtain a nonlinear algebraic system from which the post-buckling equilibrium path is determined through an iterative process.

The solutions of W and F are constructed in the form of

$$W = \sum_{m=1}^{M} a_m W_m(x,\theta) \tag{17a}$$

$$F = -\frac{\theta^2}{2}\lambda_x - \frac{x^2}{2}\lambda_\theta + \sum_{m=1}^{M} b_m F_m(x,\theta) \tag{17b}$$

where M is the number of terms in the solution series, a_m and b_m are the unknown constants to be determined, and λ_x and λ_θ are the edge forces acting on the curved and straight edges which can be determined from in-plane boundary conditions (15).

According to DQ rule, the kth partial derivative of an unknown function with respect to a coordinate, say, x, at a discrete point is approximated as the linear weighted sums of its values at all of the pre-selected sampling points along this coordinate. In this way, we have

$$\left.\frac{\partial^k (W_m, F_m)}{\partial x^k}\right|_{x=x_i} = \sum_{j=1}^{N} C_{ij}^{(k)} (W_{mj}, F_{mj}) \tag{18}$$

where N is the total number of sampling points, and $C_{ij}^{(k)}$ are the weighting coefficients that are dependent on the sampling grid only and can be calculated from recursive formulae given by Bert and Malik (1996) and Liew et al. (2001a). In this study, the sampling points are unevenly distributed in x-axis as

$$x_1 = 0.0, \quad x_2 = 0.0001, \quad x_j = \frac{1}{2}\left[1 - \cos\frac{\pi(j-2)}{N-3}\right], \quad x_{N-1} = 0.9999, \quad x_N = 1.0 \tag{19}$$

In Eq. (18), $W_{mj} = W_m(x_j,\theta)$ and $F_{mj} = F_m(x_j,\theta)$. They are to be further modeled in terms of orthogonal functions that satisfy the boundary conditions at straight edges $\theta = 0$, θ_0 and take the form of

$$F_{mj} = \sin(m+0.5)\pi\theta - \sinh(m+0.5)\pi\theta - \xi_m(\cos(m+0.5)\pi\theta - \cosh(m+0.5)\pi\theta)$$

$$\xi_m = \frac{\sin(m+0.25)\pi - \sinh(m+0.25)\pi}{\cos(m+0.25)\pi - \cosh(m+0.25)\pi} \tag{20}$$

$$\text{S–S: } W_{mj} = \sin m\pi\theta \tag{21a}$$

$$\text{C–C: } W_{mj} = F_{mj} \tag{21b}$$

$$\text{S–C: } W_{mj} = \sin(m+0.25)\pi\theta - \xi_m \sinh(m+0.25)\pi\theta, \quad \xi_m = \frac{\sin(m+0.25)\pi}{\sinh(m+0.25)\pi} \tag{21c}$$

Substitution of Eqs. (17), (18), (20), and (21) into the governing equations (6), (7) and the boundary conditions (14) and (15), and then application of the Galerkin technique leads to a set of nonlinear algebraic equations in terms of the unknown coefficients a_{mj} and b_{mj} ($m = 1,\ldots,M$, $j = 1,\ldots,N$)

$$\mathbf{G}(T,\mathbf{\Lambda})\mathbf{\Lambda} = \mathbf{\Phi}(T) \tag{22}$$

where $\mathbf{\Lambda}$ is an unknown vector which is composed of a_{mj} and b_{mj}, $\mathbf{G}$ is the nonlinear matrix that is dependent on both the temperature and $\mathbf{\Lambda}$. The right-hand side term $\mathbf{\Phi}$ comes from the thermally induced stress resultants and bending moments in simply supported boundary conditions at straight edges $\theta = 0$, θ_0, and will automatically vanish when the panel is isotropic where the stretching–bending coupling is absent, or when the panel is clamped and only displacement boundary conditions are involved. It is obvious that the bifurcational thermal buckling will take place only when $\mathbf{\Phi} = \mathbf{0}$, otherwise transverse deflection will be induced, irrespective of the magnitude of the temperature change.

The thermal buckling temperature, when it exists, is determined from the nonlinear homogeneous equation

$$\mathbf{G}(T,\boldsymbol{\Delta})\boldsymbol{\Delta}=\mathbf{0} \tag{23}$$

by an iterative numerical procedure with the following steps.

(1.1) Solve the buckling temperature ΔT_{cr} from Eq. (23) by using temperature-independent material properties, that is, the thermo-elastic properties at reference temperature T_0.
(1.2) Update $\mathbf{G}$ by using the property values at $T=T_0+\Delta T_{cr}$ to obtain a new buckling temperature.
(1.3) Repeat step (1.2) until the thermal buckling temperature converges to a prescribed error tolerance.

The nonlinear temperature–deflection curve, which is also known as the post-buckling equilibrium path, is traced by two different iterative schemes depending on the presence of $\boldsymbol{\Phi}$. When $\boldsymbol{\Phi}=\mathbf{0}$, the following iteration process is applicable:

(2.1) Begin with the dimensionless deflection $W/h=0$ at a specific point;
(2.2) Use the iterative procedures (1.1)–(1.3);
(2.3) Specify a new value of W/h;
(2.4) Calculate the thermo-elastic properties at $T=T_0+\Delta T_{cr}$, and scale up the buckling mode that is obtained in step (2.2) to form a new $\mathbf{G}$ to determine the post-buckling temperature;
(2.5) Repeat step (2.4) until the post-buckling temperature converges to a prescribed error tolerance;
(2.6) Repeat steps (2.3)–(2.5) to obtain the post-buckling equilibrium path.

The modified Newton–Raphson technique is used in case of $\boldsymbol{\Phi}\neq\mathbf{0}$, but the process is omitted here for brevity.

4. Numerical results

As there are no suitable results on the thermo-mechanical buckling and post-buckling of FGM cylindrical panels for direct comparison, thermal buckling of a clamped anti-symmetric angle-ply laminated cylindrical panel under a uniform temperature increment is solved and critical temperature results are compared in Table 1 with the existing ones obtained by Chang and Chiu (1991) as the validation of the present analysis. The material properties are temperature independent in this instance, and are given as

$$E_1/E_0=21,\quad E_2/E_0=E_3/E_0=G_{12}/E_0=1.7,\quad G_{13}/E_0=0.65,\quad G_{23}/E_0=0.639,\quad E_0=10^6\ \text{psi}$$

$$\nu_{12}=\nu_{13}=0.21,\quad \nu_{23}=0.33,\quad \alpha_1=-0.21\times10^{-6}/\text{F},\quad \alpha_2=\alpha_3=10^{-6}/\text{F}$$

The panel is fully clamped and immovable at all edges with lamination $[\pm42.5^\circ]_3$, and the geometry parameters are $L/S=1.0$, $S/R=0.25$ and $S/h=200$. Good agreement is achieved when the number of grid points

Table 1
Comparisons of buckling temperatures ΔT_{cr} (F) for a clamped antisymmetric angle-ply cylindrical panel subjected to uniform temperature change

Present				Chang and Chiu (1991)
$(M,N)=(3,9)$	$(M,N)=(5,13)$	$(M,N)=(5,15)$	$(M,N)=(7,19)$	
784.76	851.30	846.24	847.55	831.88

Table 2
Temperature-dependent thermo-elastic coefficients for silicon nitride and nickel

Thermo-elastic properties	Material	P_{-1}	P_0	P_1	P_2	P_3
E (Pa)	Silicon nitride	0	348.43e9	−3.070e−4	2.160e−7	−8.946e−11
	Nickel	0	223.95e9	−2.794e−4	3.998e−9	0
v	Silicon nitride	0	0.2400	0	0	0
	Nickel	0	0.3100	0	0	0
α (1/K)	Silicon nitride	0	5.8723e−6	9.095e−4	0	0
	Nickel	0	9.9209e−6	8.705e−4	0	0

N and the number of series terms M are increased to $(N, M) \geqslant (15, 5)$. Our solutions are slightly higher than Chang and Chiu's results because the higher order shear deformation shell theory, instead of classical shell theory, was used in their work.

Parametric studies are then conducted to supply information on both the buckling temperature and the post-buckling equilibrium paths of various FGM cylindrical shells with temperature-dependent material properties when they are subjected to axial pre-stress and uniform temperature change. Silicon nitride and nickel are chosen to be the constituent materials of the FGM panel, referred to as Si_3N_4/Ni. The temperature-dependent material constants for Young's modulus E, Poisson's ratio v and the coefficient of thermal expansion α are listed in Table 2. To highlight the effect of temperature-dependence of thermo-elastic properties, comparisons are made between the solutions using temperature-dependent and temperature-independent properties in all of the numerical examples (Tables 3, 4 and Figs. 2–9). In computation, the temperature-independent properties are (Gauthier, 1995): $E = 310$ GPa, $v = 0.24$, $\alpha = 3.4 \times 10^{-6}$ 1/K for silicon nitride and $E = 204$ GPa, $v = 0.31$, $\alpha = 13.2 \times 10^{-6}$ 1/K for nickel.

In what follows, a clockwise notation that starts from $X = 0$ is employed. "SCSC", for example, stands for a panel simply supported at edges $X = 0$, L and clamped at edges $\theta = 0$, θ_0. Three axial loading cases are considered in the analysis, i.e., (1) the panel is subjected to a tensile force (negative λ_1), (2) the panel is subjected to a compressive force (positive λ_1), and (3) the panel is free from axial force ($\lambda_1 = 0$).

The error tolerance in the iteration process is defined as the relative difference between the two consecutive solutions

Table 3
Buckling temperature parameter $\lambda_{cr} = \alpha_0 \Delta T_{cr} \times 10^3$ for clamped FGM cylindrical panels subjected to uniform axial load ($S = 0.3$ m, $L/S = 2.0$, $S/h = 100$)

Material composition	Temperature-dependent solutions		Temperature-independent solutions	
	$\lambda_1 = -200\pi^2$	$\lambda_1 = 200\pi^2$	$\lambda_1 = -200\pi^2$	$\lambda_1 = 200\pi^2$
$S/R = 0.3$				
Si_3N_4	3.1742	2.9445	3.7492	3.4393
$n = 0.5$	2.5941	2.4012	2.9739	2.7262
$n = 2.0$	2.3209	2.1373	2.6174	2.3888
$n = 10.0$	2.2018	2.0218	2.4628	2.2424
Nickel	2.0284	1.8866	2.2554	2.0829
$S/R = 0.5$				
Si_3N_4	5.9231	5.6739	7.9259	7.5118
$n = 0.5$	4.9754	4.7585	6.6366	6.0295
$n = 2.0$	4.4242	4.2225	5.5009	5.2032
$n = 10.0$	4.1417	3.9467	5.0711	4.7919
Nickel	3.9086	3.728	4.7516	4.4948

Table 4
Buckling temperature parameter $\lambda_{cr} = \alpha_0 \Delta T_{cr} \times 10^3$ for clamped FGM cylindrical panels with different in-plane boundary conditions ($S = 0.3$ m, $L/S = 2.0$, $S/h = 100$)

Material composition	Temperature-dependent solutions		Temperature-independent solutions	
	In-plane case 1	In-plane case 2	In-plane case 1	In-plane case 2
S/R = 0.3				
Si_3N_4	3.0514	2.3461	3.5828	2.6603
$n = 0.5$	2.4902	1.8536	2.8400	2.0472
$n = 2.0$	2.2242	1.6045	2.4965	1.7462
$n = 10.0$	2.1079	1.4851	2.3473	1.6041
Nickel	1.9440	1.3512	2.1525	1.4519
S/R = 0.5				
Si_3N_4	5.8074	4.5307	7.7328	5.7037
$n = 0.5$	4.8753	3.6833	6.2098	4.4444
$n = 2.0$	4.3300	3.1749	5.3613	3.7286
$n = 10.0$	4.0497	2.9027	4.9386	3.3593
Nickel	3.8248	2.7005	4.6320	3.1027

$$\varepsilon = \left| \frac{\Delta T_{cr}^{(i+1)} - \Delta T_{cr}^{(i)}}{\Delta T_{cr}^{(i)}} \right| \leqslant 10^{-4} \tag{24}$$

in the buckling analysis and

$$\varepsilon = \left| \frac{\Delta T^{(i+1)} - \Delta T^{(i)}}{\Delta T^{(i)}} \right| \leqslant 10^{-4} \tag{25}$$

in the post-buckling analysis.

Due to the stretching–bending coupling in the FGMs, only isotropic panels (the pure silicon nitride panel and the pure nickel panel) and clamped graded panels are able to exhibit bifurcation-type buckling. Tables 3 and 4 present the critical buckling temperature parameters $\lambda_{cr} = \Delta T_{cr}\alpha_0 \times 10^3$ for clamped FGM cylindrical panels ($S = 0.3$ m, $L/S = 2.0$, $S/h = 100$) with different material composition and $S/R = 0.3$,0.5, where α_0 is the thermal expansion coefficient of nickel at $T_0 = 300$ K, "Si_3N_4" and "nickel" represent isotropic silicon nitride plate and pure nickel plate respectively and $n = 0.5$, 2.0, 10.0 are the volume fraction index for graded panels. In Table 3, the panel is axially preloaded by axial tension $\lambda_1 = -200\pi^2$ or axial compression $\lambda_1 = 200\pi^2$ on edges $X = 0$, L and is immovable at other edges. In Table 4, the axial load is absent, and the results for FGM cylindrical panels with two different in-plane boundary conditions, which are refereed to as in-plane case 1 (movable at $X = 0$, L and immovable at $\theta = 0$, θ_0) and in-plane case 2 (fully immovable on all edges), are compared.

As can be seen, the temperature-independent solutions are about 9–18% higher than the temperature-dependent solutions, that is, the buckling temperature is considerably overestimated when the temperature-dependence of the material properties is not taken into consideration. Fully metallic panels (pure nickel) have the lowest buckling temperature and fully ceramic panels (pure Si_3N_4) have the largest buckling temperature. The buckling temperature decreases as the volume fraction index n increases. This is because silicon nitride has a much higher elastic modulus than nickel, and the volume percentage of silicon nitride drops sharply at larger values of n. The effect of axial tensile pre-stress is seen to enhance the thermal buckling load capacity of the panel, whereas the axial compressive load does the opposite. Moreover, the buckling temperature and the difference between the temperature-dependent and temperature-independent solutions both increase as the value of S/R becomes larger. As expected, the buckling temperature is smaller when all of the edges are fully restrained against any in-plane displacements.

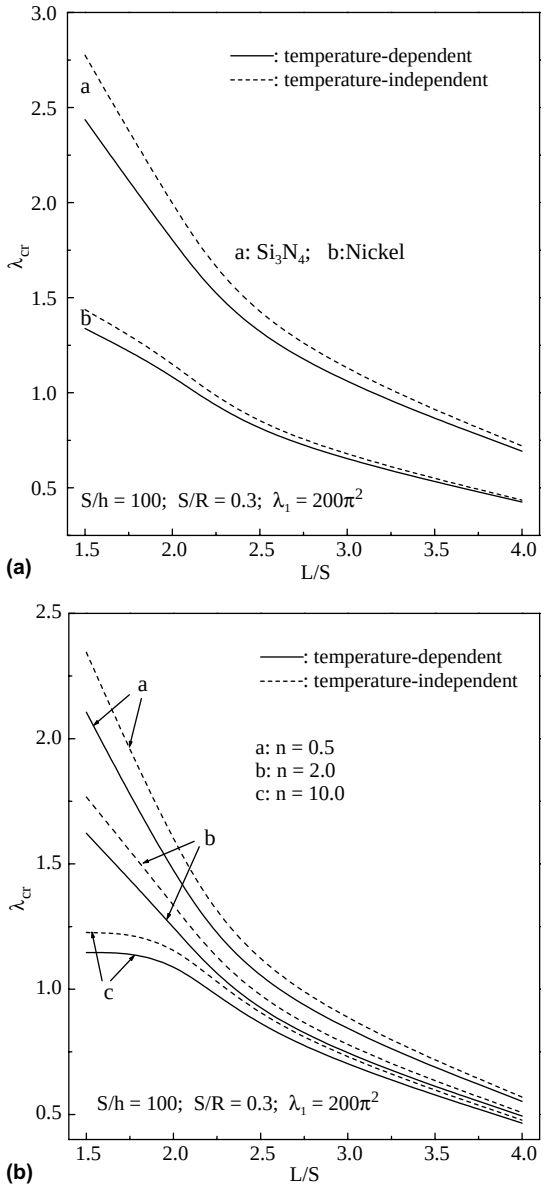

Fig. 2. Effect of L/S ratio on the buckling temperature parameter λ_{cr} for FGM cylindrical panels: (a) isotropic panels; (b) graded panels.

Fig. 2 shows the variation of the buckling temperature with varying values of L/S for axially compressed and fully clamped cylindrical panels. An increase in L/S significantly lowers both the buckling temperature and the discrepancy between the temperature-dependent and temperature-independent solutions.

Typical results for the post-buckling analysis are shown in Figs. 3–9, in which the equilibrium paths are presented for thermo-mechanically loaded FGM cylindrical panels that undergo post-buckling deformation. In these figures, w_0/h denotes the dimensionless deflection at the point $(L/2, \theta_0/2)$, $\lambda_0 = \Delta T \alpha_0 \times 10^3$ is the dimensionless temperature parameter. Unless otherwise stated, the panel is geometrically perfect,

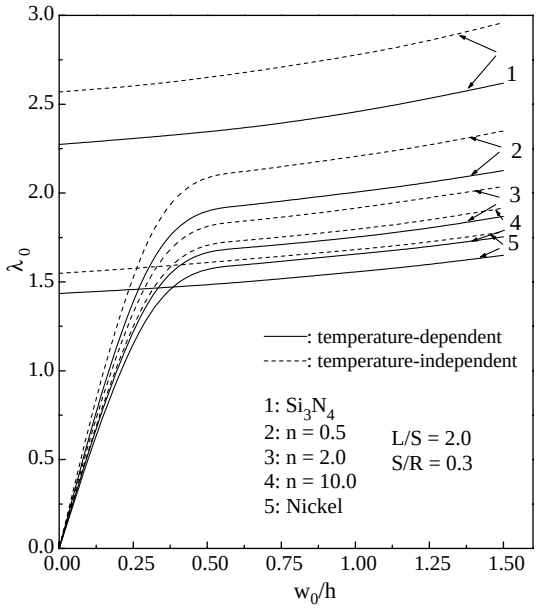

Fig. 3. Thermal post-buckling paths for simply supported FGM cylindrical panels.

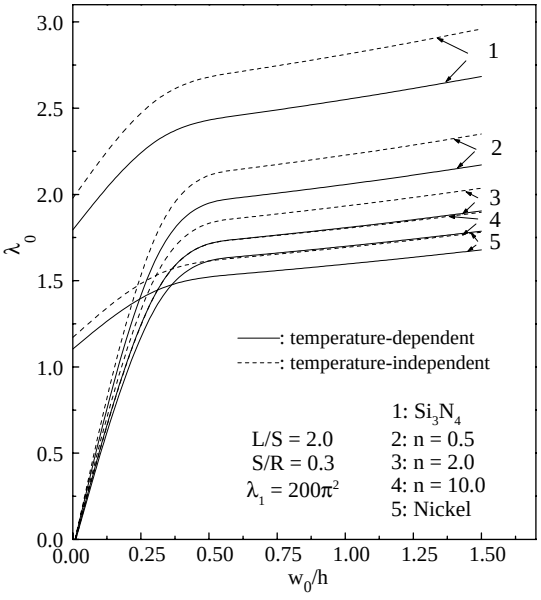

Fig. 4. Thermo-mechanical post-buckling paths for simply supported FGM cylindrical panels.

simply supported on all edges, movable at $X = 0,\ L$ and immovable at $\theta = 0,\ \theta_0$, with $L/S = 2.0$ and $S/R = 0.3$ and initially compressed by an axial force $\lambda_1 = 200\pi^2$.

Fig. 3 gives the nonlinear temperature–deflection curves for isotropic Si_3N_4 and nickel panels and the graded panels with volume fraction indices $n = 0.5$, 2.0, and 10.0 subjected to uniform temperature incre-

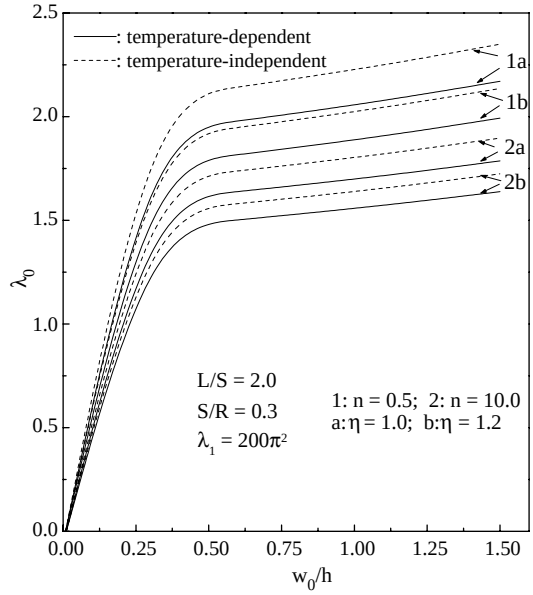

Fig. 5. Effect of imperfection on thermo-mechanical post-buckling paths for simply supported FGM cylindrical panels.

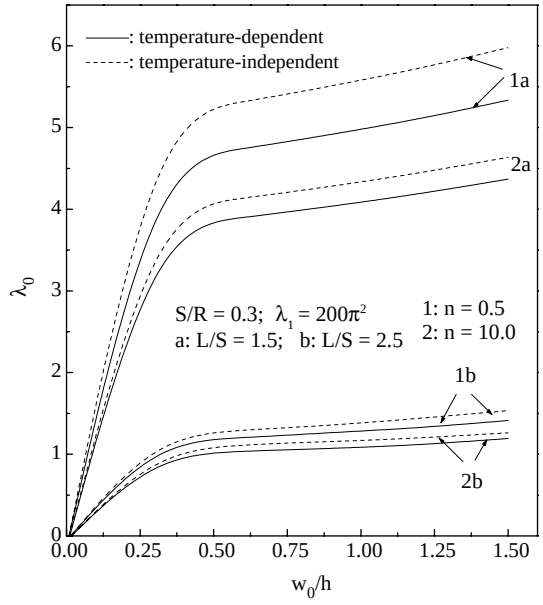

Fig. 6. Effect of L/S ratio on thermo-mechanical post-buckling paths for simply supported FGM cylindrical panels.

ment only. Fig. 4 presents the results for the same panels when they are initially stressed by axial compression λ_1. The post-buckling paths of the simply supported graded panels are not bifurcational, and in the presence of axial force, do not start from the coordinate origin due to the initial deflections induced by λ_1. As expected, the post-buckling strength is the maximum for the isotropic Si_3N_4 panel and minimum

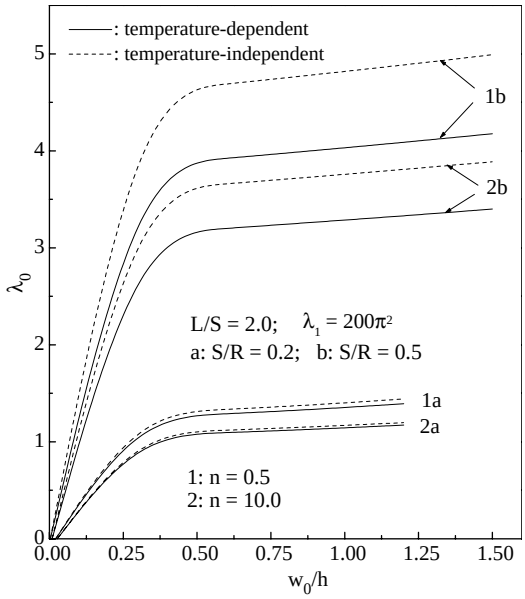

Fig. 7. Effect of S/R ratio on thermo-mechanical post-buckling paths for simply supported FGM cylindrical panels.

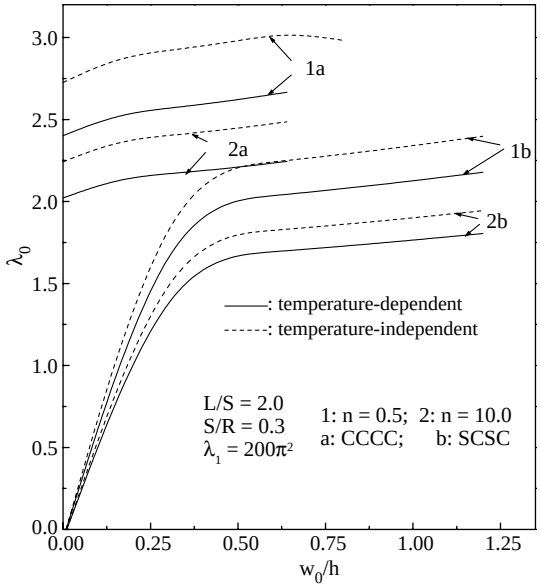

Fig. 8. Effect of out-of-plane boundary condition on thermo-mechanical post-buckling paths for FGM cylindrical panels.

for the pure nickel panel and degrades as the volume fraction index n increases. The post-buckling equilibrium path becomes lower when the temperature-dependent properties are taken into account. Moreover, the application of an initial axial load makes the curves for isotropic panels in Fig. 4 somewhat different from those in Fig. 3 at small deflections ($w_0/h \leqslant 0.45$–0.5).

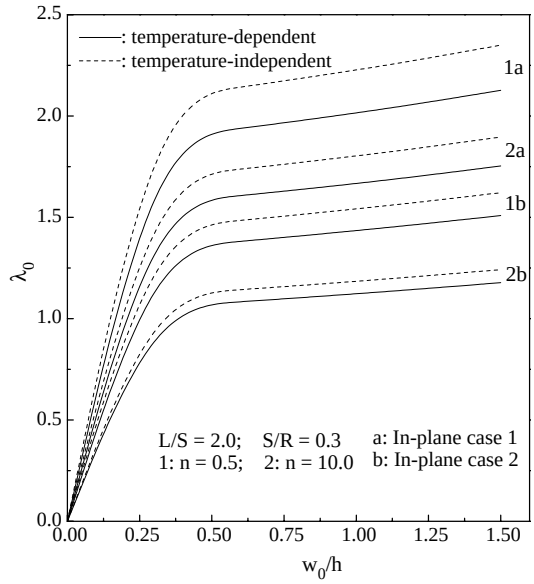

Fig. 9. Effect of in-plane boundary condition on thermal post-buckling paths for simply supported FGM cylindrical panels.

Fig. 5 evaluates the effect of geometric imperfection on the thermo-mechanical post-buckling equilibrium paths of graded FGM cylindrical panels with $n = 0.5$ and 10.0. For the sake of simplicity, the initial geometric imperfection W^* is assumed to have the same shape as the additional deflection W and the imperfection parameter is defined as $\eta = 1 + 2\frac{W^*}{W}$. This parameter is taken to be $\eta = 1.2$ for the imperfect panels in this example. It is noted that in the presence of geometric imperfection the post-buckling equilibrium path becomes lower.

The thermo-mechanical post-buckling behavior of FGM cylindrical panels with varying ratio of L/S is compared in Fig. 6, in which curves 1a, 2a and 1b, 2b are the equilibrium paths for the cases of $L/S = 1.5$ and 2.5, respectively. The results show that the post-buckling strength declines significantly as L/S increases.

The effect of flatness on the thermo-mechanical post-buckling behavior of FGM cylindrical panels is shown in Fig. 7 by comparing the post-buckling temperature–deflection curves of panels with length-to-radius ratios $S/R = 0.2$ and $S/R = 0.5$. The results show that the equilibrium path is very sensitive to panel flatness. The panel with a flatted configuration (smaller length-to-radius ratio) has a much lower buckling temperature and post-buckling curves than the one with a greater length-to-radius ratio.

Fig. 8 gives the thermo-mechanical post-buckling temperature–deflection relationships for FGM cylindrical panels with CCCC and SCSC boundary conditions. The post-buckling equilibrium paths for the fully clamped panel are of bifurcation type, whereas those for the SCSC panels are not. The post-buckling temperature difference between the temperature-dependent and temperature-independent solutions of the CCCC panels is bigger than that of the SCSC panels. Moreover, the CCCC panel has greater post-buckling load-carrying capacity than its SCSC counterpart.

It is observed that in both Figs. 7 and 8, curves 1a and 2a stop at lower values of w_0/h. This is because the post-buckling paths cannot be traced beyond those values due to the convergence problem in the iteration process, indicating that the post-buckling paths do not exist when w_0/h is larger than those values.

The influence of in-plane boundary condition is displayed in Fig. 9 by comparing the thermal post-buckling equilibrium paths for FGM cylindrical panels with two types of in-plane displacement constraints.

The results demonstrate that the panels with one pair of movable edges (in-plane case 1) have much higher post-buckling load-carrying capacity than those immovable on all edges (in-plane case 2). This can be expected, as greater thermally induced compressive stresses will develop in the fully immovable panels, which significantly weaken the structure stiffness.

5. Conclusions

The buckling and post-buckling behavior of cylindrical panels that are comprised of functionally graded materials with temperature-dependent material properties and are subjected to a combination of an axial force and a uniform temperature change have been investigated within the framework of the classical shell theory with von-Karman–Donnell-type of kinematic nonlinearity. The material properties are assumed to be the nonlinear function of temperature and graded in the thickness direction. The effect of initial geometric imperfection is also included in the analysis. A semi-analytical approach, together with an iterative algorithm, is used as a nonlinear solution scheme to determine the critical buckling temperature and the post-buckling temperature–deflection curves. The results show that both the buckling temperature and the equilibrium path in the post-buckling regime are significantly over-predicted when the temperature-dependence of the material properties is not taken into consideration. It is also confirmed that the buckling and post-buckling behaviors of FGM cylindrical panels are greatly influenced by the volume fraction index, the axial pre-stress, the out-of-boundary conditions, initial geometric imperfection, and panel configuration.

Acknowledgements

The work described in this paper is fully supported by research grant from the Research Grants Council of the Hong Kong Special Administrative Region, China (Project No. CityU 1139/04E). The authors are grateful for this financial support.

References

Aboudi, J., Pindera, M.J., Arnold, S.M., 1997. Microstructural optimization of functionally graded composites subjected to a thermal gradient via the coupled higher-order theory. Composites Part B: Engineering 32B, 93–108.

Argyris, J., Tenek, L., 1995. Postbuckling of composite laminates under compressive load and temperature. Computer Methods in Applied Mechanics and Engineering 128, 49–80.

Bert, C.W., Malik, M., 1996. Differential quadrature method in computational mechanics: A review. Applied Mechanics Reviews ASME 49, 1–28.

Birman, V., 1997. Stability of functionally graded shape memory alloy sandwich panels. Smart Materials and Structures 6, 278–286.

Chang, J.S., Chiu, W.C., 1991. Thermal buckling analysis of antisymmetric laminated cylindrical shell panels. International Journal of Solids and Structures 27, 1295–1309.

Chen, L.W., Chen, L.Y., 1989. Thermal buckling behavior of laminated composite plates with temperature-dependent properties. Composite Structures 13, 275–287.

Deng, K.S., Ji, Z., Davies, A.W., Williams, F.W., 2000. Thermal buckling of axially precompressed cylindrical shells irradiated by laser beam. AIAA Journal 38, 1789–1794.

Feldman, E., 1996. The effect of temperature-dependent material properties on elasto-viscoplastic buckling behaviour of non-uniformly heated MMC plates. Composite Structures 35, 65–74.

Gauthier, M.M. (Ed.), 1995. Engineering Materials Handbook, Desk Edition. ASM International, USA.

Javaheri, R., Eslami, M.R., 2002. Thermal buckling of functionally graded plates. AIAA Journal 40, 162–169.

Kitipornchai, S., Yang, J., Liew, K.M., 2004. Semi-analytical solution for nonlinear vibration of laminated FGM plates with geometric imperfections. International Journal of Solids and Structures 41, 2235–2257.

Koizumi, M., 1993. The concept of FGM. Ceramic Transactions, Functionally Gradient Materials 34, 3–10.
Lee, J., 2001. Effects of temperature-dependent physical properties on the response of thermally postbuckled plates. Journal of Thermal Stresses 24, 1117–1135.
Liew, K.M., Teo, T.M., Han, J.B., 2001a. Three-dimensional static solutions of rectangular plates by variant differential quadrature method. International Journal of Mechanical Sciences 43, 1611–1628.
Liew, K.M., He, X.Q., Ng, T.Y., Sivashanker, S., 2001b. Active control of FGM plates subjected to a temperature gradient: Modelling via finite element method based on FSDT. International Journal for Numerical Methods in Engineering 52, 1253–1271.
Liew, K.M., He, X.Q., Ng, T.Y., Kitipornchai, S., 2002. Active control of FGM shells subjected to a temperature gradient via piezoelectric sensor/actuator patches. International Journal for Numerical Methods in Engineering 55, 653–668.
Liew, K.M., Kitipornchai, S., Zhang, X.Z., Lim, C.W., 2003a. Analysis of the thermal stress behavior of functionally graded hollow circular cylinders. International Journal of Solids and Structures 40, 2355–2380.
Liew, K.M., Yang, J., Kitipornchai, S., 2003b. The postbuckling of piezoelectric FGM plates subjected to thermo-electro-mechanical loading. International Journal of Solids and Structures 40, 3869–3892.
Liew, K.M., Yang, J., Kitipornchai, S., 2004. Thermal postbuckling of laminated plates comprising FGM with temperature-dependent material properties. Journal of Applied Mechanics ASME 71, 839–850.
Ma, L.S., Wang, T.J., 2003. Nonlinear bending and post-buckling of a functionally graded circular plate under mechanical and thermal loadings. International Journal of Solids and Structures 40, 3311–3330.
Morimoto, T., Tanigawa, Y., Kawamura, R., 2003. Thermal buckling analysis of inhomogeneous rectangular plate due to uniform heat supply. Journal of Thermal Stresses 26, 1151–1170.
Na, K.S., Kim, J.H., 2004. Three-dimensional thermal buckling analysis of functionally graded materials. Composites Part B: Engineering 35, 429–437.
Ng, T.Y., He, X.Q., Liew, K.M., 2002. Finite element modeling of active control of functionally graded shells in frequency domain via piezoelectric sensors and actuators. Computational Mechanics 28, 1–9.
Noda, N., 1999. Thermal stresses in functionally graded materials. Journal of Thermal Stresses 22, 477–512.
Noor, A.K., Burton, W.S., 1992a. 3-dimensional solutions for the thermal buckling and sensitivity derivatives of temperature-sensitive multilayered angle-ply plates. Journal of Applied Mechanics ASME 59, 848–856.
Noor, A.K., Burton, W.S., 1992b. Computational models for high temperature multilayered plates and shells. Applied Mechanics Reviews ASME 45, 419–446.
Reddy, J.N., 2000. Analysis of functionally graded plates. International Journal for Numerical Methods in Engineering 47, 663–684.
Reddy, J.N., Cheng, Z.Q., 2001. Three-dimensional thermomechanical deformations of functionally graded rectangular plates. European Journal of Mechanics A—Solids 20, 841–855.
Reddy, J.N., Chin, C.D., 1998. Thermomechanical analysis of functionally graded cylinders and plates. Journal of Thermal Stresses 21, 593–626.
Shahsiah, R., Eslami, M.R., 2003. Thermal buckling of functionally graded cylindrical shells. Journal of Thermal Stresses 26, 277–294.
Shen, H.S., 2001. Thermal postbuckling behavior of imperfect shear deformable laminated plates with temperature-dependent properties. Computer Methods in Applied Mechanics and Engineering 190, 5377–5390.
Shen, H.S., 2002a. Postbuckling analysis of axially-loaded functionally graded cylindrical panels in thermal environment. International Journal of Solids and Structures 39, 5991–6010.
Shen, H.S., 2002b. Postbuckling analysis of axially-loaded functionally graded cylindrical shells in thermal environment. Composites Science and Technology 62, 977–987.
Shen, H.S., 2003. Postbuckling analysis of pressure-loaded functionally graded cylindrical shells in thermal environments. Engineering Structures 25, 487–497.
Shen, H.S., 2004. Thermal postbuckling behavior of functionally graded cylindrical shells with temperature-dependent properties. International Journal of Solids and Structures 41, 1961–1974.
Shen, H.S., Leung, A.Y.T., 2003. Postbuckling of pressure-loaded functionally graded cylindrical panels in thermal environments. Journal of Engineering Mechanics ASCE 129, 414–425.
Singha, M.K., Ramachandra, L.S., Bandyopadhyay, J.N., 2003. Thermomechanical postbuckling response and first-ply failure analysis of doubly curved panels. AIAA Journal 41, 2486–2491.
Sofiyev, A.H., 2004. The stability of functionally graded truncated conical shells subjected to aperiodic impulsive loading. International Journal of Solids and Structures 41, 3411–3424.
Tanigawa, Y., 1995. Some basic thermoelastic problems for nonhomogeneous structural materials. Applied Mechanics Reviews 48, 377–389.
Touloukian, Y.S., 1967. Thermophysical Properties of High Temperature Solid Materials. MacMillan, New York.
Vel, S.S., Batra, R.C., 2002. Exact solution for thermoelastic deformations of functionally graded thick rectangular plates. AIAA Journal 40, 1421–1433.

Woo, J., Meguid, S.A., Liew, K.M., 2003. Thermomechanical postbuckling analysis of functionally graded plates and shallow cylindrical shells. Acta Mechanica 165, 99–115.

Yang, J., Kitipornchai, S., Liew, K.M., 2003. Large amplitude vibration of thermo-electro-mechanically stressed FGM laminated plates. Computer Methods in Applied Mechanics and Engineering 192, 3861–3885.

Yang, J., Kitipornchai, S., Liew, K.M., 2004a. Nonlinear analysis of thermo-electro-mechanical behavior of shear deformable FGM plates with piezoelectric actuators. International Journal for Numerical Methods in Engineering 59, 1605–1632.

Yang, J., Liew, K.M., Kitipornchai, S., 2004b. Dynamic stability of laminated FGM plates based on higher-order shear deformation theory. Computational Mechanics 33, 305–315.

Yang, J., Shen, H.S., 2003a. Nonlinear bending analysis of shear deformable functionally graded plates subjected to thermo-mechanical loads and under various boundary conditions. Composites Part B: Engineering 34, 103–115.

Yang, J., Shen, H.S., 2003b. Parametric resonance of shear deformable functionally graded cylindrical panels in thermal environment. Journal of Sound and Vibration 261, 871–893.